Light propagation in binary kagome ribbons with evolving disorder

A. Radosavljević, G. Gligorić, P. P. Beličev, A. Maluckov, and M. Stepić
P Group, Vinča Institute of Nuclear Sciences, University of Belgrade, P.O. Box 522, 11001 Belgrade, Serbia*
(Received 3 March 2017; published 26 July 2017)

By introducing evolving disorder in the binary kagome ribbons, we study the establishment of diffusive spreading of flat band states characterized by diffractionless propagation in regular periodic ribbons. Our numerical analysis relies on controlling strength and rate of change of disorder during light propagation while tailoring binarism of the kagome ribbons in order to isolate the flat band with the gap from the rest of the ribbon's eigenvalue spectrum and study systematically its influence on diffusion. We show that the flat band plays a dominant role in the establishment of the diffusion for a given strength and rate of change of disorder, whereas the rest of the ribbon's eigenvalue spectrum induces only quantitative differences in the light spreading regimes. Due to the universality of studied phenomena, our findings may be of interest in various disordered physical systems with flat spectral bands, ranging from photonics to ultracold matter systems and plasmonics.

DOI: 10.1103/PhysRevE.96.012225

I. INTRODUCTION

Stationary (quenched) disorder plays a fundamental role in wave dynamics, resulting in a complete halt of wave transport due to consecutive destructive interferences of waves scattered from randomly distributed scatterers. This universal effect of wave localization is known as Anderson localization (AL) [1]. So far, AL has been studied in solid state [2,3], optical [4–10], acoustic [11], and matter wave systems [12,13]. Nonstationary (nonquenched or evolving) disorder instead breaks the coherence necessary for achieving AL, yielding normal or anomalous diffusive expansion of a wave packet [14–17]. In order for AL to take place, wave interactions also have to be absent from a disordered system since even weak interactions can inhibit AL giving rise to a subdiffusive spreading of the wave packet [18–20].

Among different wave systems, photonic lattices (PLs) have emerged as the key experimental setup to study AL [4–8] and other wave packet related effects [21–23]. In PLs, evolution of the initially launched light waves can be observed along the light propagation direction simply using a CCD camera [23]. Moreover, owing to the fast-developing fabrication techniques, such as femtosecond laser inscription [7,24] or optical induction [25,26], it is possible to fabricate PLs with a desired geometrical arrangement and refractive indices of waveguides. High precision and controllability of available fabrication techniques enabled demonstration of AL in two-dimensional (2D) and one-dimensional (1D) PLs with random refractive indices of waveguides which are "frozen" along the light propagation direction [4–7]. Moreover, conditions for the observation of AL can be disturbed in a controllable manner which allows for experimental investigation of the mechanism behind the destruction of AL. For example, the nonlinear response of PLs can easily be induced by increasing the intensity of the input light beam [27] which was used in attempts to experimentally study the mutual effect of the light wave interactions and the quenched disorder (QD) on the light propagation [4,5]. Additionally, advanced fabrication processes also enabled investigation of the light spreading regimes under the influence of evolving disorder (ED) in PLs with controllable disordered refractive index profiles of waveguides in both transverse and light propagation directions. It has been demonstrated that an initially launched narrow light beam can expand at the faster than ballistic rate under certain circumstances [28].

Most of the experimental studies of AL in the quenched disordered PLs and its degradation in the presence of the nonlinearity or ED have been conducted in conventional disordered 1D and 2D PLs. These PLs are conventional in the sense that the disordered potential is superimposed on the underlying periodic potential which renders dispersive eigenvalue spectrum except for certain points in momentum space where local derivatives are zero [29]. These realizations of the quenched disordered systems correspond to the original disordered model introduced by Anderson [1]. When exciting a periodic PL with the corresponding dispersive eigenvalue spectrum, using a narrow light beam, a set of linear extended states with different propagation constants will be excited. Excited states propagate incoherently along the PL, and the initially narrow light beam spreads across the PL forming a pattern of discrete diffraction [29]. In such PLs, QD suppresses the diffraction of the narrow light beam through the mechanism of AL. However, different underlying periodic arrangements of waveguides in PLs, which dictate the eigenvalue spectra of PLs, can significantly influence the light localization induced by the superimposed QD. This leads to a new direction in studying the disordered systems. A particularly interesting situation arises when one or more bands in the eigenvalue spectrum are completely flat. States corresponding to the flat band (FB), so called flat band states (FBSs), represent a set of degenerated linear compact localized states with zero tails occupying only several PL sites. FBSs as well as any linear combination of them propagate without diffraction along the FB PLs, which have been confirmed experimentally in a number of FB PL models, such as the Lieb [30,31], kagome [32], rhombic or diamond [33], and sawtooth PLs [34]. This feature makes FB PLs good candidates for all-optical coherent image transmission at low powers [35,36], for instance. Since FBSs are localized already in the linear periodic FB PLs, the question is which role QD plays in the FBSs' propagation. So far, this question has been addressed in several studies of the light localization in various quenched disordered quasi-1D and 2D PLs hosting one or more FBs [37–40]. It has been shown that QD lifts the degeneracy of FBSs. As far as the localization of the states originating from the FB in the disordered FB systems

is concerned, it has been observed that it depends on the position of the FBs with regard to the neighboring dispersive bands of the FB PL's eigenvalue spectrum [37,38]. The main finding of the recent studies is the emergence of different eigenvalue-dependent scaling laws for localization lengths with disorder strength, dependent on a mutual position of the flat and the dispersive spectral bands [37,38]. However, most of these studies lack a more detailed analysis of the localization dynamics of the states originating from the FB in FB PLs with QD.

Beside extensive studies of the light localization in different FB PL models with the QD, some efforts have also been made towards understanding the effects of the mutual influence of the nonlinearity and the QD on the light propagation in FB PLs [39]. Motivated by the recent studies of the light localization in FB PLs with the QD, we wanted to investigate whether the presence of a FB and its position in the spectrum with regard to dispersive bands also influences the light diffusion in FB PLs with ED. Having this in mind, we study in detail FBSs' propagation in linear uniform and binary kagome ribbons (KRs) [41] with QD and ED. Uniform KRs represent quasi-1D FB PLs, obtained by dimensional reductions of 2D kagome PLs [42]. Binary KRs are formed by embedding additional different periodicities in the uniform KRs [41], which enables the formation of a gap around the FB, thus isolating it from the rest of the eigenvalue spectra of the KRs.

This paper is organized as follows. We begin with Sec. II by introducing the tight binding model used to describe the light beam evolution in the uniform and binary KRs with QD or ED. In Sec. III, the localization in the linear uniform and binary KRs with QD is studied and compared with existing studies of various FB PL models with QD. In Sec. IV we comparatively investigate the behavior of FBS propagation in KRs with QD and ED with the accent on ED. We perform an extensive investigation of the FBS spreading dynamics in KRs with the ED while controlling its change rate along the light propagation direction and its strength. The main objectives are to study the role of the FB in establishing the diffusive spreading in KRs with ED by exciting it with a FBS and to find a relation between FBS spreading in the presence of the ED and FBS localization when disorder is quenched. Results are compared with the narrow light beam propagation in the conventional PLs with ED. Finally, Sec. V concludes the paper with a summary of our results.

II. MODEL OF DISORDERED BINARY KAGOME RIBBONS

In Ref. [41] we studied two types of discrete binary KRs: the binary kagome ladder and the binary kagome strip. Here we will consider only the binary kagome ladder which will be referred to as the binary KR in the following. The schematic of the binary KR with its characteristic six-site cell is shown in Fig. 1(a). The thick solid lines denote the strong linear coupling strength between neighboring sites V_2, whereas the dashed ones stand for weak coupling strength V_1.

The light propagation in the discrete linear binary KRs along the light propagation (evolving) direction z may be described by the following set of dimensionless differential-

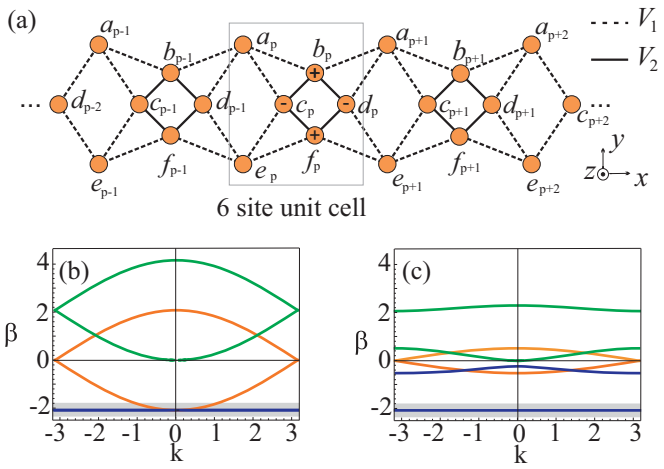

FIG. 1. (a) Binary KR. A unit cell that contains six sites. The FBS is a compact localized state which occupies four sites with the π phase change between adjacent sites represented by + and − signs. The eigenvalue's spectra reduced to the first Brillouin zone in (b) uniform and (c) binary KRs for $V = 0.25$. The bands in (c), formed due to the splitting of the corresponding bands in the uniform case (b), are depicted with the same color [41]. The gray areas around the FB illustrate its smearing in the KRs with quenched disorder.

difference equations in the tight binding approximation:

$$
\begin{aligned}
i\,\partial_z a_p &= \varepsilon_p^a a_p + V_1(b_{p-1} + b_p) + V_1 c_p + V_1 d_{p-1},\\
i\,\partial_z b_p &= \varepsilon_p^b b_p + V_1(a_{p+1} + a_p) + V_2 c_p + V_2 d_p,\\
i\,\partial_z c_p &= \varepsilon_p^c c_p + V_1 a_p + V_2 b_p + V_1 e_p + V_2 f_p,\\
i\,\partial_z d_p &= \varepsilon_p^d d_p + V_1 a_{p+1} + V_2 b_p + V_1 e_{p+1} + V_2 f_p,\\
i\,\partial_z e_p &= \varepsilon_p^e e_p + V_1 c_p + V_1 d_{p-1} + V_1(f_{p-1} + f_p),\\
i\,\partial_z f_p &= \varepsilon_p^f f_p + V_2 c_p + V_2 d_p + V_1(e_{p+1} + e_p),
\end{aligned}
\tag{1}
$$

where $a_p(z)$, $b_p(z)$, $c_p(z)$, $d_p(z)$, $e_p(z)$, and $f_p(z)$ represent amplitudes of the light beam at the individual site of the six-site unit cell in the binary KRs [Fig. 1(a)]. Indices $p = 1,\ldots,N$ stand for unit cell index, whereas N is the total number of unit cells in the ribbons. Terms ε_p^x $(x = a,b,c,d,e,f)$ represent the on-site lattice potential.

We consider the on-site QD and ED, which are modeled by assigning uniformly distributed random numbers from a given range of $[-W/2,W/2]$ to the terms ε_p^x. Parameter W is the disorder strength. In the case of QD, values of ε_p^x are fixed along the light propagation direction, whereas in the case of ED they are changed in regular intervals. In general, ε_p^x can be presented in a form

$$
\varepsilon_p^x = \sum_{j=0}^{j=n_z} \varepsilon_{pj}^x \{\theta(z + j\,\Delta z) - \theta[z + (j+1)\Delta z]\}, \tag{2}
$$

where Δz is the interval after which values of ε_p^x are changed in the propagation direction (step of change in the disorder realizations), $n_z = L/\Delta z$ is the total number of disorder realizations along evolution direction z, L is the propagation length, and θ is the Heaviside function. For each j, ε_{pj}^x is a different set of uniform random numbers from the interval $[-W/2,W/2]$. In this way, we keep the disorder strength

W fixed during its evolution along z. When decreasing step Δz, disorder changes faster in the light propagation direction. Therefore, the rate of change in disorder is proportional to $1/\Delta z$. This realization of the ED corresponds to the experimental realization in Ref. [28] and the model used in Ref. [43] and can be interpreted as stacking different KRs with QD of length Δz in the light propagation direction z. In such circumstances, QD can be interpreted as a limiting case of ED for $\Delta z = L$.

Eigenvalues and eigenstate profiles can be found assuming the solution for the electric field of the light beam in the standard form

$$\{a_p(z),b_p(z),c_p(z),d_p(z),e_p(z),f_p(z)\} = \{A,B,C,D,E,F\}\exp(-i\beta z)\exp(ikp), \quad (3)$$

where k stands for the transverse Bloch wave vector of the binary KRs, β is the propagation constant of the observed state, and $\{A,B,C,D,E,F\}$ is the steady state (z independent) profile of the considered wave field. In the case of regular periodic KRs, one can set $\varepsilon_p^x = 0$ without loss of generality. When the coupling constants are equal ($V_1 = V_2 = v$), the KRs are noted as uniform in Ref. [41]. The eigenvalue spectrum of the periodic uniform KR consists of three linear bands, given by the following expressions:

$$\begin{aligned}\beta_1 &= 2v[1+\cos(k/2)],\\ \beta_2 &= 2v\cos(k/2),\\ \beta_3 &= -2v.\end{aligned} \quad (4)$$

The lowest band is flat, and it touches higher dispersive bands at the center of the Brillouin zone [Fig. 1(b)]. Degenerated four-site compact localized states corresponding to FB (FBSs) can be represented as

$$\{a_p,b_p,c_p,d_p,e_p,f_p\} = \{0,1,-1,-1,0,1\}\delta_{p,p_0}\exp(-i\beta_3 z), \quad (5)$$

when they occupy sites coupled by V_2 [Fig. 1(a)] or

$$\{a_p,b_p,c_p,d_{p-1},e_p,f_p\} = \{1,0,-1,-1,1,0\}\delta_{p,p_0}\exp(-i\beta_3 z), \quad (6)$$

when they occupy sites coupled by V_1. Here, δ stands for the Kronecker δ function equal to 1 for certain cell index p_0.

Introducing binarism ($V_1 \neq V_2$), additional gaps within the eigenvalue spectrum open for $V_1 < 1$ and $V_2 = 1$ [Fig. 1(c)]. The largest one forms around FB, isolating it from the rest of the spectrum. Width w_g of the widest gap is proportional to the ratio of coupling constants $V = V_1/V_2$ as $w_g(V) \backsim 2(1-V)$. The ratio V will be referred to as the coupling ratio in the following. Decreasing the value of V below $V = 1$, introduced binarism increases, and the gap around FB widens. In the case of the periodic binary KRs, FBSs can only occupy sites coupled by stronger coupling constants V_2 (see Ref. [41]). Let us note that in the presence of disorder terms the uniform and binary lattices will be used only to indicate to which lattice structure the disordered potential is added.

In KRs with QD, the states originating from the FB are no longer degenerated and have corresponding eigenvalues in the range of width W around the FB [Figs. 1(b) and 1(c)]. For simplicity, the states originating from the FB in the disordered KRs will be called disordered FBSs as in Refs. [37,38]. Depending on the coupling ratio V, the FB can touch the higher dispersive zone (uniform KRs, $V = 1$) or be isolated from it (binary KRs, $V < 1$). In the first case, even weak disorder causes mixing of FBSs with dispersive states. It has been shown that in such cases the corresponding disordered FBSs have a sparse structure with a finite number of peaks and an increasing distance between them as disorder weakens [37]. If $V < 1$, the width of the gap around the FB effectively decreases with disorder. Therefore, we expect to observe two different situations: If the disorder is weak enough, the smeared FB stays isolated from the dispersive band, whereas the strong disorder closes the gap around the FB and causes mixing of the FB with the dispersive band, similar to the case of uniform KRs with QD. It has been shown that in the case of weak disorder, for the FB positioned in the gap, the disordered FBSs behave similarly to defect states and are evanescent on a length set by the gap width [38].

In order to characterize the light propagation in the disordered KRs and compare it with the existing studies of a disordered FB and conventional PLs, we use standard measures: the participation ratio [44,45] to measure the number of strongly excited sites,

$$P = \frac{1}{\sum_{p=1}^{N}(|a_p|^4+|b_p|^4+|c_p|^4+|d_p|^4+|e_p|^4+|f_p|^4)}, \quad (7)$$

the second moment, which gives information about the width of the light field distribution or information about the distance between tails of the light field distribution [39],

$$\begin{aligned}m_2 = \sum_{p=1}^{N}\Bigg[&[X(z)-p]^2(|a_p|^2+|e_p|^2)\\ &+\left(X(z)-p-\frac{1}{4}\right)^2|c_p|^2\\ &+\left(X(z)-p-\frac{1}{2}\right)^2(|b_p|^2+|f_p|^2)\\ &+\left(X(z)-p-\frac{3}{4}\right)^2|d_p|^2\Bigg],\end{aligned} \quad (8)$$

where $X(z)$ is the first moment (center of mass) calculated as

$$\begin{aligned}X(z) = \sum_{p=1}^{N}\Bigg[&p(|a_p|^2+|e_p|^2)+\left(p+\frac{1}{4}\right)|c_p|^2\\ &+\left(p+\frac{1}{2}\right)(|b_p|^2+|f_p|^2)+\left(p+\frac{3}{4}\right)|d_p|^2\Bigg],\end{aligned} \quad (9)$$

and the localization length ξ. The localization length is related to the exponential decay of the localized light beam's amplitude with the distance from the light beam's centrum as $\exp(-1/\xi)$. It gives the impression of the volume occupied by the light beam since the amplitude of the localized beam practically decays to zero after the distance equal to one localization length. The localization length is calculated for different values of parameters V and W applying the standard

transfer matrix method to map equations derived from system (1) [46,47]. The procedure for the determination of ξ can be summarized in several steps. Here we are interested in the properties of the FBSs. Thus, the system of Eqs. (1) is transformed into the map equations at the energy manifold $E = E_{\mathrm{FB}}$. The light beam propagation therefore is described by a map trajectory, i.e., flow at the energy manifold. In order to calculate the localization length, one first needs to calculate Liapunov exponents which represent the rates of divergence of map trajectory from the E_{FB} manifold [48]. The localization length is proportional to the inverse of the least positive Liapunov exponent. A detailed theoretical explanation of the relation between the Liapunov exponents and the localization length as well as numerical procedures for calculation of Liapunov exponents can be found in Ref. [48].

III. LOCALIZATION OF FLAT BAND STATES IN KAGOME RIBBONS WITH QUENCHED DISORDER

Here, features of localized states originating from the FB in the KRs with QD are studied. In order to characterize the disordered FBSs for different values of parameters V and W, we start by numerically diagonalizing the system of Eqs. (1) with the disordered terms ε_p^x for the KRs with a finite number of unit cells N after assuming the solution for the electric field of the light beam in the form given by expression (3). Figures 2(a) and 2(b) show the saturable values of the participation numbers and the second moments, whereas Fig. 2(c) displays the localization lengths of the disordered FBSs for different values of coupling ratio V and disorder strength W. The presented results are averaged after repeating calculations for 200 realizations of the uniform and binary KRs with QD.

In the case of the uniform KRs with QD, saturable values of the participation numbers clearly show that the disordered FBSs occupy more waveguides than the FBSs in the regular uniform KRs, even for very low disorder strengths W [red circles in Fig. 2(a)]. Saturable values of m_2 indicate that the disordered FBSs are not zero tailed [red circles in Fig. 2(b)] as opposed to the FBSs in the regular uniform KRs. It can be noted that both saturable P and m_2 do not change significantly with weak disorder ($W < 0.1$). However, the localization length increases when weakening disorder as $\xi(W) \backsim W^{-1/2}$ [red circles in Fig. 2(c)]. Therefore, the disordered FBSs in the weakly disordered uniform KRs are sparse states with a finite, almost constant, number of peaks and nonzero tails. Since these states spread over longer lengths when disorder weakens, it yields that distance between their peaks increases. Our results are in agreement with the previous studies of the localization of the disordered FBSs in PLs which host intersecting flat and dispersive bands. Moreover, the scaling law of the localization length with disorder is exactly the same as predicted in the studies of spectrally similar disordered FB PLs [37]. Disordered FBSs in such PLs have different features from Anderson localized states in the conventional PLs, which are single-peaked exponentially localized states with the localization length changing more rapidly with the disorder W as $\xi(W) \backsim W^{-2}$ [39]. For the disorder strength above $W = 0.1$, all analyzed measures of the localization of the disordered FBSs decrease when increasing disorder, indicating that the localized disordered FBSs start to resemble the standard Anderson localized states.

Saturable values of P and m_2 for all studied disordered binary KRs for $W < 1$ [pink, green, and blue triangles in Figs. 2(a) and 2(b)] show that the disordered FBSs in the binary KRs occupy almost the same number of waveguides as the FBSs in the regular binary KRs but acquire nonzero tails which grow when increasing disorder. For a given disorder strength, tails are longer for higher V. The localization length for $W < 1$ keeps a constant finite value set by the width of the gap which isolates the FB from the higher dispersive zone [pink, green, and blue triangles in Fig. 2(c)]. Our results are in agreement with the predictions presented in Refs. [38,39].

For very high disorder ($W > 1$), the gaps around the FB close, and the influence of binarism becomes "erased." Therefore, values of all analyzed localization measures tend to be similar in the disordered uniform and binary KRs for $W > 1$ (Fig. 2).

In order to investigate the dynamics of the localization of the disordered FBSs, we study the propagation of an initially excited single FBS through the disordered KRs. We solve numerically the system of Eqs. (1) with periodic boundary conditions applying the Runge-Kutta method of the sixth order [49] and assuming initial conditions that correspond to the single four-site FBS excitation [expression (5)]. Using the solutions of the system (1), we calculate P and m_2 along z. Averaged results for $P(z)$ and $m_2(z)$ along the disordered uniform and binary KRs with the coupling ratio $V = 0.25$ are shown in Fig. 3. Results are averaged after performing calculations for 100 realizations of the disordered KRs. The coupling ratio $V = 0.25$ is chosen to secure that the gap around the FB stays open for all studied values of disorder strength W.

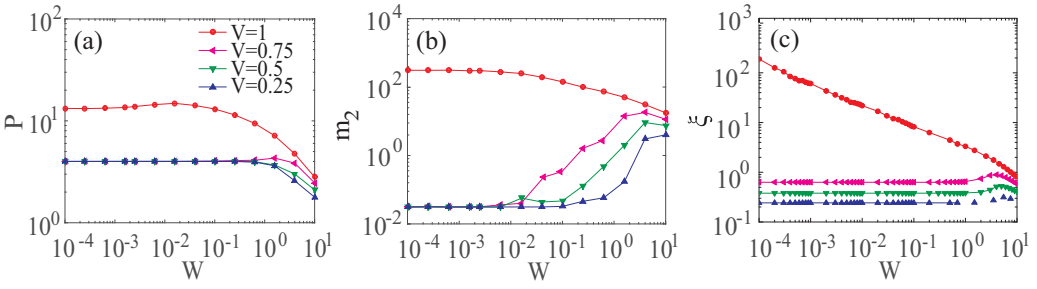

FIG. 2. Saturable values of (a) the participation number and (b) the second moment of the disordered FBSs in the uniform and binary KRs for different disorder strengths W. (c) The dependence of the localization length of the disordered FBSs in the uniform and binary KRs on disorder strength W. All figures are given on the log-log scale.

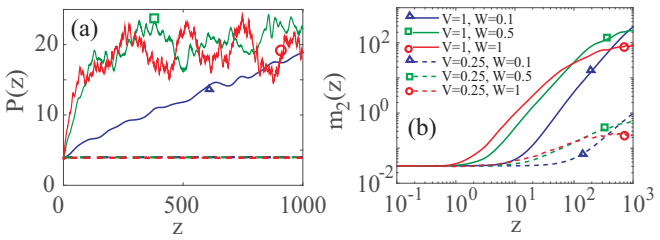

FIG. 3. (a) The participation number and (b) the second moment of the FBS during propagation in the uniform and binary KRs with QD. The second moments are presented on the log-log scale.

Lengths of all KRs with QD are fixed at $L = 1000$ for easier comparison with results for the FBS propagation in the KRs with ED, which are presented in the next section.

As expected, both $P(z)$ and $m_2(z)$ show that diffractionless propagation of the initially excited FBS is destroyed when QD is introduced in the uniform and binary KRs. In the case of the uniform KRs with medium ($W = 0.5$) and strong ($W = 1$) QDs, we observe that $P(z)$ and $m_2(z)$ saturate to values that correspond to the saturable values in Figs. 2(a) and 2(b) after a certain distance in the z direction, indicating that the localization occurred. The distances in z, after which the initially excited FBS becomes localized due to QD, shortening when increasing the disorder strength and may be referred to as the transient regime. For weak disorder ($W = 0.1$) we do not observe saturation of P and m_2 during propagation for $L = 1000$ [the solid lines in Figs. 3(a) and 3(b)] since the propagation length L is shorter than the localization length. Therefore, the mode dynamics is transient in that case.

Contrary to the case of the uniform KRs with QD, in the case of disordered binary KRs we do not observe long transient regimes which depend on the disorder strength. The number of strongly excited ribbon sites stays almost constant along z and around the value that corresponds to the number of initially excited four sites by FBS excitation [the dashed lines in Fig. 3(a)]. The dashed lines in Fig. 3(b) show that m_2 of the excited FBS slightly increases during propagation for all W, which is in accordance with Fig. 2(b).

The localization length dependence on W presented in Fig. 2(c) can be a relevant measure for the observed dynamics of the FBS in the KRs with QD. In the case of the uniform KRs with QD, ξ decays when increasing disorder [red circles in Fig. 2(c)]. Therefore, the FBS has to settle to a localized state by spreading over a shorter distance when increasing disorder. This means shorter transient regimes. In the case of the disordered binary KRs, ξ of the localized state to which the excited FBS settles is independent of the disorder strength and much shorter than ξ obtained in the case of the uniform KRs with QD [compare red circles and blue triangles in Fig. 2(c)].

IV. PROPAGATION OF FLAT BAND STATES IN KAGOME RIBBONS WITH EVOLVING DISORDER

In the following, we investigate the spreading of the initially excited single compact localized state—FBS [expression (5)] in KRs with ED. In order to classify diffusive spreading of the FBS for different coupling ratios, strengths, and evolution steps of ED, we express the second moment in a form [50]

$$m_2(z) \backsim z^{\alpha}. \tag{10}$$

Diffusion types can be classified based on the growth rate α of the second moment [51]. Normal diffusion is characterized by $\alpha = 1$, whereas the following nomenclature is used throughout the literature for anomalous diffusion $\alpha \neq 1$: subdiffusion for $\alpha < 1$ and superdiffusion for $\alpha > 1$. For the special case of $\alpha = 2$, notation ballistic spreading is used instead of superdiffusion, whereas for $\alpha > 2$ superdiffusive spreading is noted as faster than ballistic spreading [50,51].

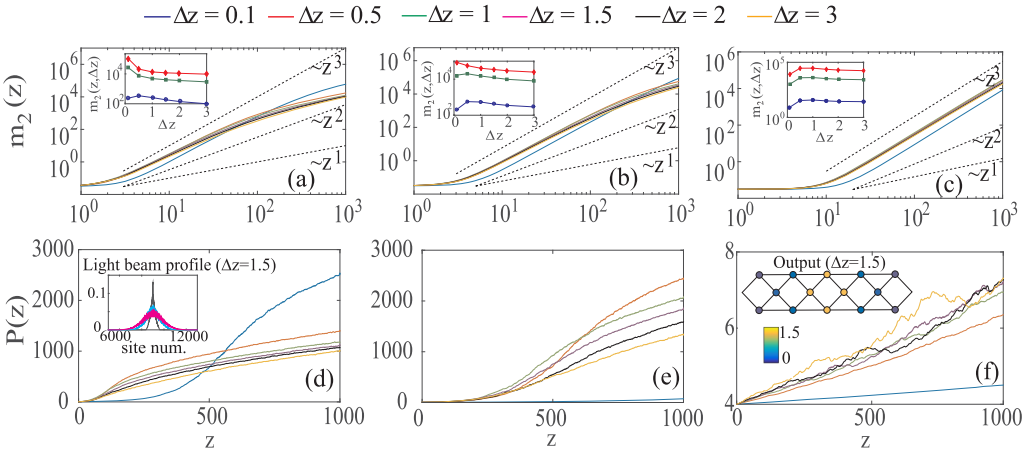

FIG. 4. The second moment and the participation number along the uniform KRs with ED for different evolution steps Δ_z and disorder strengths (a) and (d) $W = 1$, (b) and (e) $W = 0.5$, and (c) and (f) $W = 0.1$. The insets in (a)–(c) show values of m_2 as a function of Δz at different points along the light propagation direction: $z = 100$ (blue circles), $z = 500$ (green squares), and $z = 1000$ (red diamonds). The inset in (d) illustrates the light field profile at three different points along the propagation directions $z = 100$ (gray line), $z = 500$ (light blue line), and $z = 1000$ (magenta line) during diffusive spreading of the initially launched single FBS in the strongly disordered uniform KRs with $W = 1$ for $\Delta z = 1.5$. The inset in (f) shows the distribution of the light field amplitudes at the output of the KRs with $W = 0.1$ for $\Delta z = 1.5$. The second moments are presented on the log-log scale. The dashed straight lines with slopes 3,2, and 1, respectively, are guiding lines for the estimation of the growing rates of the m_2 curves.

In Fig. 4 the averaged results for $m_2(z)$ and $P(z)$ along the uniform KRs with ED for $W = 1$ [Figs. 4(a) and 4(d)], $W = 0.5$ [Figs. 4(b) and 4(e)], and $W = 0.1$ [Figs. 4(c) and 4(f)] are shown. For each W, we investigate FBS propagation using the same steps $\Delta z = \{0.1, 0.5, 1, 1.5, 2, 3\}$. In order to ensure the compactness of the results and the long time limit conditions for studying the regimes of diffusive spreading, the chosen values for Δz are much longer than the numerical integration step and much shorter than the system length $\Delta z \ll L$.

For strong disorder ($W = 1$), both $m_2(z)$ and $P(z)$ grow along z when disorder changes [Figs. 4(a) and 4(d)], as opposed to the case of QD when $m_2(z)$ and $P(z)$ saturate [red solid lines in Figs. 3(a) and 3(b)]. Values of $m_2(z)$ and $P(z)$ reached at the output of the uniform KRs with ED for all Δz are significantly higher than the saturable values of $m_2(z)$ and $P(z)$ in the uniform KRs with QD. Moreover, it can be seen that the second moments at the output of PLs with ED $m_2(z = L)$ monotonically decrease when increasing Δz [red diamonds in the inset in Fig. 4(a)]. Extracted values of the growth rates of $m_2(z)$ gradually decrease along z for every Δz. For the propagation lengths $L = 1000$ set in our simulations, the growth rate settles to $\alpha = 1.4$ for a short evolution step ($\Delta z = 0.1$), indicating that FBS spreading can be classified as superdiffusion. For longer steps ($\Delta z > 0.1$), growth rates settle to $\alpha = 1.1$, showing that the diffusive spreading of the initially launched FBS becomes more similar to normal diffusion in these cases. The light beam profiles keep Gaussian shapes for every Δz during propagation, which is illustrated in the inset of Fig. 4(d) for randomly chosen $\Delta z = 1.5$ at three different points along z. It should be noted that the initial FBS excitation is compact, but during propagation in the presence of strong ED it acquires tails and eventually takes Gaussian shape.

In the case of weak ED ($W = 0.1$), $m_2(z)$ grows with almost constant growth rates along z [Fig. 4(c)], which are estimated to be in the range of $\alpha = [2.8, 3]$ for different Δz. Behaviors of $m_2(z)$ indicate faster than ballistic spreading according to the classification in Ref. [50]. From values of $m_2(z)$ at several points along z given in the inset of Fig. 4(c), it can be observed that, for the same propagation length, the second moment reaches the highest value for a certain Δz.

In the uniform KRs with weak ED, numbers of occupied sites do not increase significantly for any Δz from the initial value of $P = 4$, which corresponds to FBS excitation [Fig. 4(f)]. It can be concluded that only the tails of the light beam spread fast whereas most of the light energy stays around initially excited sites. Typical distribution of the light field amplitudes observed at the output of the uniform KRs with weak ED is given in the inset of Fig. 4(f) for randomly chosen $\Delta z = 1.5$. Values of $P(z = L)$ at the output of uniform KRs with ED are lower than $P(z = L)$ reached in the case of QD with the same strength. Since each chosen step $\Delta z \ll \xi$ [see the blue solid lines in Figs. 3(a) and 3(b)], weak ED slows down the spreading of FBS excitation before it "fills" the localization volume and establishes a different regime of spreading.

In the case of intermediate ED strength ($W = 0.5$) [Figs. 4(b) and 4(e)], the propagation of the FBS can be similar to the case of weak or to the case of strong disorder depending on Δz. For longer steps ($\Delta z > 0.1$), the FBS spreads superdiffusively with the growth rates of $m_2(z)$ settled at $\alpha = 1.5$, similar to the case of the strong ED with $\Delta z = 0.1$. For short steps ($\Delta z = 0.1$), the growth rate of $m_2(z)$ is $\alpha = 2.5$. In this case, the FBS spreading resembles the spreading of the FBS in the uniform KRs with the weak ED ($W = 0.1$) for which the growth rates of $m_2(z)$ indicate faster than ballistic spreading. However, the behavior of $P(z)$ indicates a small increase in the number of ribbon sites occupied by tails of light beams along z.

Next, we focus on the the binary KRs with the low coupling ratio of $V = 0.25$ in order to keep the gap around the smeared FB open for all studied values of the disorder strength. We

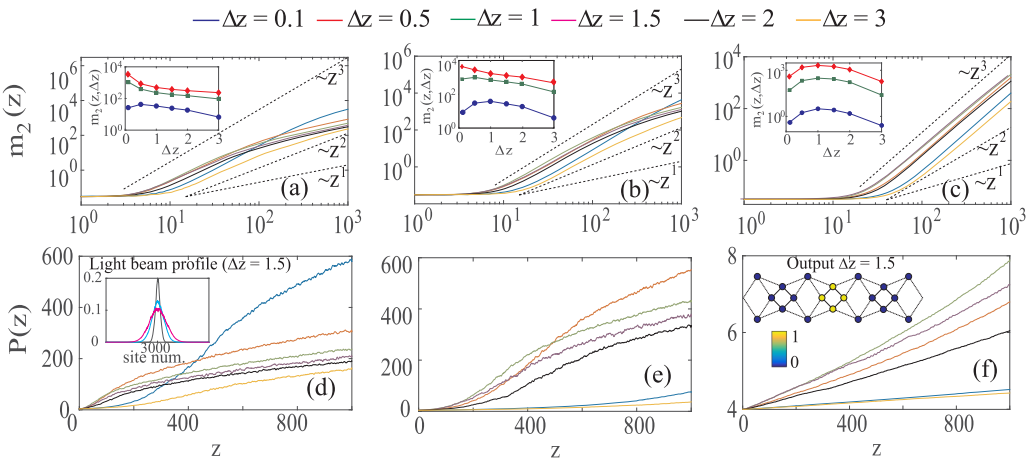

FIG. 5. The second moment and the participation number along binary KRs with ED for different evolution steps Δz and disorder strengths (a) and (d) $W = 1$, (b) and (e) $W = 0.5$, and (c) and (f) $W = 0.1$. The coupling ratio of binary KRs is $V = 0.25$. The insets in (a)–(c) show values of m_2 as a function of Δz at different points along the light propagation direction: $z = 100$ (blue circles), $z = 500$ (green squares), and $z = 1000$ (red diamonds). The inset in (d) illustrates the light field profile at three different points along propagation directions $z = 100$ (gray line), $z = 500$ (light blue line), and $z = 1000$ (magenta line) for the case of diffusive spreading of the initially launched single FBS for $W = 1$ and $\Delta z = 1.5$. The inset in (f) shows the distribution of the light field amplitudes at the output of KRs with $W = 0.1$ for $\Delta z = 1.5$. The second moments are presented on the log-log scale. The dashed straight lines with slopes 3, 2, and 1, respectively, are guiding lines for the estimation of the growing rates of the m_2 curves.

investigate the propagation of FBS excitation for the same steps of disorder change and disorder strengths as in the case of the uniform KRs with ED. In Fig. 5 averaged $m_2(z)$ and $P(z)$ along the binary KRs with the ED for $W = 1$ [Figs. 5(a) and 5(d)], $W = 0.5$ [Figs. 5(b) and 5(e)], and $W = 0.1$ [Figs. 5(c) and 5(f)] are shown.

Interestingly, for given W and Δz we observe the same regimes of FBS propagation in the uniform and the binary KRs with ED. Quantitative differences in the growth rates of $m_2(z)$ for the same W and Δz in the uniform and in the binary KRs are negligible. However, $m_2(z)$ and $P(z)$ reach higher values in the uniform KRs than in the binary KRs with ED for the same propagation length of $L = 1000$. Exceptions are the values for $P(z)$ in the case of weak ED, which are almost the same for the FBS propagating in the uniform and in the binary KRs. Since our realization of ED relies on changing the disordered on-site potential abruptly after steps Δz, we interpreted it as stacking KRs of length Δz, each with different QD potentials, in the light propagation direction. Therefore, figuratively speaking, light which propagated in one KR with QD as a superposition of its eigenstates, reaches the next KR with different realization of QD which further modulates a light beam supporting the propagation of different eigenstates with respect to the previous KR, and so on.

Here, we briefly comment on the possibility to associate the observed FBSs spreading properties in the disordered binary KRs with a dephasing efficiency of the ED following the approach in Ref. [50]. The FBSs are eigenstates of the regular KRs. In our paper and in literature [37,38], it is shown that the implementation of the on-site quenched disorder differently affects the FBSs' propagation with respect to the degree of isolation of the corresponding FB from the rest of the system's eigenvalue spectrum. The controlling parameter here is the coupling ratio V. The isolation of the FB is associated with the changes in a behavior of the FBSs in the KR with QD. This can be related to the finding that in the binary KR ($V \neq 1$) for the fixed value of V, the localization length ξ is independent of the W value and much shorter than the localization length in the case of uniform KRs with QD, Fig. 2(c).

To interpret the FBSs' propagation properties in the KR with on-site ED, we assume that the ED induces hopping between different eigenstates of the KR's parts with QD [50]. The coupling then is driven by the frequency components of the ED spectrum that are resonant with the energy differences between the eigenstates. The influence of the ED on the propagation of the FBSs can be associated with the overlap between two spectra: the eigenstates density spectrum of the KRs and the corresponding spectrum of the ED [50]. The eigenstates' density spectra of the KRs with $V = 1$ (uniform) and $V = 0.25$ (binary) in the presence of the QD with $W = 0.1$, 0.5, and 1 are schematically presented in Fig. 6(a).

The distributions of the eigenstates' densities around the FB in the uniform KR with on-site QD are characterized by higher amplitudes at the FB position than those in the binary KR with QD. On the other hand, the eigenstates' distribution in the binary KRs is characterized by the occurrence of gaps which are wider in the lattices with a smaller value of V. Therefore, the overlap with the ED spectrum in the area around the FB is more pronounced in the uniform case. Roughly, the latter can be sketched as the higher probability for resonant

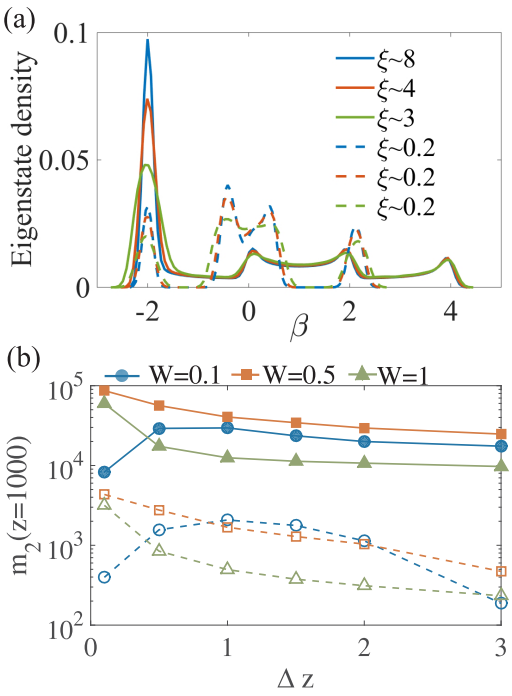

FIG. 6. (a) The eigenstates density spectrum [$\rho(\beta)$ vs β] of the KRs with QD. The solid lines denote the uniform KR case ($V = 1$), whereas the dashed lines denote the binary KR ($V = 0.25$). The blue, red, and green lines correspond to the fixed values of the disorder strength: $W = 0.1$, 0.5, and 1, respectively. The corresponding values of ξ are shown in the figure. (b) The $m_2(z = 1000)$ vs Δz for uniform (solid lines with solid symbols) and binary (dashed lines with open symbols) lattices with respect to $W = 0.1$, 0.5, and 1.

excitation of the eigenstates from this area in uniform than in the binary KRs with ED. The interplay of the mentioned effects, the efficiency of the dephasing by the ED, and the localization of states induced by the QD might be associated with observed behavior of the second moment m_2 of the FBSs [50], Fig. 6(b). The $m_2(z = 1000)$ vs Δz curves in the uniform lattice are above the ones in the binary KRs for each selected value of W. This can be related with the value of ξ and more efficient dephasing in the KR with $V = 1$ than with $V \neq 1$. The shapes of the m_2 vs Δz curves in the uniform and binary KRs for each particular value of W are similar. Moreover, it can be noted that the dephasing induced by the ED smears out the differences between the spreading tendencies of the FBSs with respect to the coupling ratios of $V = 1$ and $V \neq 1$.

Finally, we may summarize that the presented results imply that, for a given propagation length, normal or anomalous diffusion of initially excited FBSs in both uniform and binary KRs with ED can be observed depending on the strength and the evolution step of the disorder. The insets of Figs. 4(a)–4(c) and 5(a)–5(c) show the changes in functional dependence of the second moment along z on Δz, which are a consequence of the decreasing growth rates of $m_2(z)$ along z. The same $m_2(z, \Delta z)$ dependence can be observed for both weak and strong EDs but after shorter propagation distance in the case of strong ED. This can be related to the observation that the diffusion rates found for the KRs with weak ED appear as transient rates of the FBS spreading in the presence of strong

ED. On the other hand, the last can be used to guess that, for any disorder strength, the FBS spreading in the presence of ED tends to settle to the normal diffusive spreading in the long time (propagation) limit. The confirmation of our assumption is a challenging task for further investigations.

V. CONCLUSIONS

The study presented here is a step forward in understanding the influence of disorder on the light propagation in the FB systems. We investigate the role of the FB and its position with respect to the dispersive bands in the eigenvalue spectrum of FB PLs on the propagation of the FBSs in the presence of ED.

We consider binary KRs, which allow us to control the position of the FB with regard to the rest of the eigenvalue spectrum by controlling the coupling ratio V. KRs are modeled by the system of differential-difference equations in the tight binding approximation. The influence of on-site disorder is investigated, which is kept frozen in the case of QD or changed in regular intervals in the propagation direction in the case of ED. We observe that, in the uniform KRs with QD, the localization length of the disordered FBS scales with the disorder strength as $\xi(W) \backsim W^{-1/2}$ whereas it remains constant in the case of the binary KRs with QD, in accordance with the previous studies [37–40].

Our analysis of the FBS propagation in the uniform and binary KRs with ED yields that for a given observation length L, normal or anomalous diffusion can be observed, depending on the strength and the rate of change in the ED. The same regimes of diffusive spreading are observed in the uniform and binary KRs with the ED under the same conditions. Mixing of the FB with the rest of the PL's spectrum in the uniform KRs causes only quantitative differences in the FBS spreading dynamics. This peculiar dynamics indicates that the spreading of the FBSs in the presence of the ED is not significantly affected by the interplay of the dispersive-extended states. In order to relate the localization of the FBSs in the presence of the QD and FBSs' spreading regimes in the presence of the ED, we have adopted the approach based on the perturbation theory in Ref. [50].

Although our results are discussed in the context of PLs, they can be relevant for any system in which FB structures can be realized, such as optical lattices for trapping of ultracold atoms [52,53] or metallic lattices for obtaining a flat plasmonic band [54].

ACKNOWLEDGMENTS

The authors acknowledge support from the Swedish-Chilean-Serbian trilateral project "Control of light and matter waves propagation and localization in photonic lattices" from the Swedish Research Council within the Swedish Research Links programme, Grant No. 348-2013-6752 and the Ministry of Education, Science and Technological Development of the Republic of Serbia (Project No. III 45010).

[1] P. W. Anderson, Absence of diffusion in certain random lattices, Phys. Rev. **109**, 1492 (1958).
[2] P. A. Lee and T. V. Ramakrishnan, Disordered electronic systems, Rev. Mod. Phys. **57**, 287 (1985).
[3] M. L. Williams and H. J. Maris, Numerical study of phonon localization in disordered systems, Phys. Rev. B **31**, 4508 (1985).
[4] T. Schwartz, G. Bartal, S. Fishman, and M. Segev, Transport and Anderson localization in disordered two-dimensional photonic lattices, Nature (London) **446**, 52 (2007).
[5] Y. Lahini, A. Avidan, F. Pozzi, M. Sorel, R. Morandotti, D. N. Christodoulides, and Y. Silberberg, Anderson Localization and Nonlinearity in One-Dimensional Disordered Photonic Lattices, Phys. Rev. Lett. **100**, 013906 (2008).
[6] Y. Lahini, R. Pugatch, F. Pozzi, M. Sorel, R. Morandotti, N. Davidson, and Y. Silberberg, Observation of a Localization Transition in Quasiperiodic Photonic Lattices, Phys. Rev. Lett. **103**, 013901 (2009).
[7] S. Ghosh *et al.*, Ultrafast laser inscribed waveguide lattice in glass for direct observation of transverse localization of light, Appl. Phys. Lett. **100**, 101102 (2012).
[8] L. Martin *et al.*, Anderson localization in optical waveguide arrays with off-diagonal coupling disorder, Opt. Express **19**, 13636 (2011).
[9] D. S. Wiersma, P. Bartolini, A. Lagendijk, and R. Righini, Localization of light in a disordered medium, Nature (London) **390**, 671 (1997).
[10] T. Sperling, W. Bührer, C. M. Aegerter, and G. Maret, Direct determination of the transition to localization of light in three dimensions, Nat. Photonics **7**, 48 (2013).
[11] H. Hu, A. Strybulevych, J. H. Page, S. E. Skipetrov, and B. A. van Tiggelen, Localization of ultrasound in a three-dimensional elastic network, Nat. Phys. **4**, 945 (2008).
[12] J. Billy *et al.*, Direct observation of Anderson localization of matter waves in a controlled disorder, Nature (London) **453**, 891 (2008).
[13] G. Roati *et al.*, Anderson localization of a non-interacting Bose–Einstein condensate, Nature (London) **453**, 895 (2008).
[14] J.-P. Bouchaud and A. Georges, Anomalous diffusion in disordered media: Statistical mechanisms, models and physical applications, Phys. Rep. **195**, 127 (1990).
[15] D. A. Steck, V. Milner, W. H. Oskay, and M. G. Raizen, Quantitative study of amplitude noise effects on dynamical localization, Phys. Rev. E **62**, 3461 (2000).
[16] C. D'Errico, M. Moratti, E. Lucioni, L. Tanzi, B. Deissler, M. Inguscio, G. Modugno, M. B. Plenio, and F. Caruso, Quantum diffusion with disorder, noise and interaction, New J. Phys. **15**, 045007 (2013).
[17] Y. Krivolapov, L. Levi, S. Fishman, M. Segev, and M. Wilkinson, Super-diffusion in optical realizations of Anderson localization, New J. Phys. **14**, 043047 (2012).
[18] S. Flach, D. O. Krimer, and C. Skokos, Universal Spreading of Wave Packets in Disordered Nonlinear Systems, Phys. Rev. Lett. **102**, 024101 (2009).
[19] M. Larcher, F. Dalfovo, and M. Modugno, Effects of interaction on the diffusion of atomic matter waves in one-dimensional quasiperiodic potentials, Phys. Rev. A **80**, 053606 (2009).
[20] M. Larcher *et al.*, Subdiffusion of nonlinear waves in quasiperiodic potentials, New J. Phys. **14**, 103036 (2012).

[21] R. Morandotti, U. Peschel, J. S. Aitchison, H. S. Eisenberg, and Y. Silberberg, Experimental Observation of Linear and Nonlinear Optical Bloch Oscillations, Phys. Rev. Lett. **83**, 4756 (1999).
[22] I. L. Garanovich, S. Longhi, A. A. Sukhorukov, and Y. S. Kivshar, Light propagation and localization in modulated photonic lattices and waveguides, Phys. Rep. **518**, 1 (2012).
[23] F. Lederer *et al.*, Discrete solitons in optics, Phys. Rep. **463**, 1 (2008).
[24] G. Della Valle, R. Osellame, and P. Laporta, Micromachining of photonic devices by femtosecond laser pulses, J. Opt. A: Pure Appl. Opt. **11**, 013001 (2009).
[25] N. K. Efremidis, S. Sears, D. N. Christodoulides, J. W. Fleischer, and M. Segev, Discrete solitons in photorefractive optically induced photonic lattices, Phys. Rev. E **66**, 046602 (2002).
[26] B. Terhalle, *Controlling Light in Optically Induced Photonic Lattices*, Springer Thesis: Recognizing Outstanding Ph.D. Research (Springer, Berlin, 2011).
[27] G. P. Agrawal, *Nonlinear Fiber Optics*, 4th ed. (Academic, New York 2007).
[28] L. Levi, Y. Krivolapov, S. Fishman, and M. Segev, Hyper-transport of light and stochastic acceleration by evolving disorder, Nat. Phys. **8**, 912 (2012).
[29] H. S. Eisenberg, Y. Silberberg, R. Morandotti, and J. S. Aitchison, Diffraction Management, Phys. Rev. Lett. **85**, 1863 (2000).
[30] R. A. Vicencio, C. Cantillano, L. Morales-Inostroza, B. Real, C. Mejía-Cortés, S. Weimann, A. Szameit, and M. I. Molina, Observation of Localized States in Lieb Photonic Lattices, Phys. Rev. Lett. **114**, 245503 (2015).
[31] S. Mukherjee, A. Spracklen, D. Choudhury, N. Goldman, P. Öhberg, E. Andersson, and R. R. Thomson, Observation of a Localized Flat-Band State in a Photonic Lieb Lattice, Phys. Rev. Lett. **114**, 245504 (2015).
[32] Y. Zong, S. Xia, L. Tang, D. Song, Y. Hu, Y. Pei, J. Su, Y. Li, and Z. Chen, Observation of localized flat-band states in Kagome photonic lattices, Opt. Express **24**, 8877 (2016).
[33] S. Mukherjee and R. R. Thomson, Observation of localized flat-band modes in a quasi-one-dimensional photonic rhombic lattice, Opt. Lett. **40**, 5443 (2015).
[34] S. Weimann, L. Morales-Inostroza, B. Real, C. Cantillano, A. Szameit, and R. A. Vicencio, Transport in Sawtooth photonic lattices, Opt. Lett. **41**, 2414 (2016).
[35] R. A. Vicencio and C. Mejía-Cortés, Diffraction-free image transmission in kagome photonic lattices, J. Opt. **16**, 015706 (2014).
[36] S. Xia, Y. Hu, D. Song, Y. Zong, L. Tang, and Z. Chen, Demonstration of flat-band image transmission in optically induced Lieb photonic lattices, Opt. Lett. **41**, 1435 (2016).
[37] S. Flach, D. Leykam, J. D. Bodyfelt, P. Matthies, and A. S. Desyatnikov, Detangling flat bands into Fano lattices, Europhys. Lett. **105**, 30001 (2014).
[38] D. Leykam, J. D. Bodyfelt, A. S. Desyatnikov, and S. Flach, Localization of weakly disordered flat band states, Eur. Phys. J. B **90**, 1 (2017).
[39] D. Leykam, S. Flach, O. Bahat-Treidel, and A. S. Desyatnikov, Flat band states: Disorder and nonlinearity, Phys. Rev. B **88**, 224203 (2013).
[40] D. Leykam, Wave and spectral singularities in photonic lattices, Doctoral dissertation, The Australian National University, 2015.
[41] P. P. Beličev, G. Gligorić, A. Radosavljević, A. Maluckov, M. Stepić, R. A. Vicencio, and M. Johansson, Localized modes in nonlinear binary kagome ribbons, Phys. Rev. E **92**, 052916 (2015).
[42] R. A. Vicencio and M. Johansson, Discrete flat-band solitons in the kagome lattice, Phys. Rev. A **87**, 061803(R) (2013).
[43] A. Radosavljević, G. Gligorić, A. Maluckov, M. Stepić, and D. Milović, Light propagation management by disorder and nonlinearity in one-dimensional photonic lattices, J. Opt. Soc. Am. B **30**, 2340 (2013).
[44] T. Zhu and E. Ertekin, Phonons, localization, and thermal conductivity of diamond nanothreads and amorphous graphene, Nano Lett. **16**, 4763 (2016).
[45] T. Zhu and E. Ertekin, A generalized Debye-Peierls/Allen-Feldman model for the lattice thermal conductivity of low dimensional and disordered materials, Phys. Rev. B **93**, 155414 (2016).
[46] D. O. Krimer and S. Flach, Statistics of wave interactions in nonlinear disordered systems, Phys. Rev. E **82**, 046221 (2010).
[47] B. Kramer and A. MacKinnon, Localization: theory and experiment, Rep. Prog. Phys. **56**, 1469 (1993).
[48] A. J. Lichtenberg and M. A. Lieberman, *Regular and Chaotic Dynamics*, second ed. (Springer-Verlag, New York, 1992).
[49] W. H. Press, S. A. Teukolsky, W. T. Vetterling, and B. P. Flannery, *Numerical Recipes The Art of Scientific Computing*, 3rd ed. (Cambridge University Press, New York, 2007).
[50] M. Moratti, Transport phenomena in disordered time-dependent potentials, Doctoral dissertation, Università degli Studi di Firenze, 2014.
[51] R. Balescu, *Statistical Dynamics: Matter out of Equilibrium* (Imperial College Press, London, 1997).
[52] J. Ruostekoski, Optical Kagome Lattice for Ultracold Atoms with Nearest Neighbor Interactions, Phys. Rev. Lett. **103**, 080406 (2009).
[53] G.-B. Jo, J. Guzman, C. K. Thomas, P. Hosur, A. Vishwanath, and D. M. Stamper-Kurn, Ultracold Atoms in a Tunable Optical Kagome Lattice, Phys. Rev. Lett. **108**, 045305 (2012).
[54] Y. Nakata, T. Okada, T. Nakanishi, and M. Kitano, Observation of flat band for terahertz spoof plasmon in metallic kagomé lattice, Phys. Rev. B **85**, 205128 (2012).